Article

Synthesis and Characterization of Cellulose Acetate Membranes with Self-Indicating Properties by Changing the Membrane Surface Color for Separation of Gd(III)

Oana Steluta Serbanescu [1], **Andreea Madalina Pandele** [1,2], **Florin Miculescu** [3] and **Stefan Ioan Voicu** [1,2,*]

[1]   Department of Analytical Chemistry and Environmental Engineering, Faculty of Applied Chemistry and Materials Science, Gheorghe Polizu 1-7, 011061 Bucharest, Romania; oana.sserbanescu@yahoo.com (O.S.S.); pandele.m.a@gmail.com (A.M.P.)

[2]   Advanced Polymers Materials Group, Gheorghe Polizu 1-7, 011061 Bucharest, Romania

[3]   Faculty of Materials Science, University Politehnica of Bucharest, Splaiul Independentei 313, 060042 Bucharest, Romania; f_miculescu@yahoo.com

*   Correspondence: svoicu@gmail.com or stefan.voicu@upb.ro; Tel.: +40-721165757

check for updates

Abstract: This study presents a new, revolutionary, and easy method for evaluating the separation process through a membrane that is based on changing the color of the membrane surface during the separation process. For this purpose, a cellulose acetate membrane surface was modified in several steps: initially with amino propyl triethoxysilane, followed by glutaraldehyde reaction and calmagite immobilization. Calmagite was chosen for its dual role as a molecule that will complex and retain Gd(III) and also as an indicator for Gd(III). At the contact with the membrane surface, calmagite will actively complex and retain Gd(III), and it will change the color of the membrane surface during the complexation process, showing that the separation occurred. The synthesized materials were characterized by Fourier transform infrared spectroscopy (FT-IR), thermal analysis (TGA-DTA), X-ray photoelectron spectroscopy (XPS), and Raman spectroscopy, demonstrating the synthesis of membrane material with self-indicating properties. In addition, in the separation of the Gd(III) process, in which a solution of gadolinium nitrate was used as a source and as a moderator in nuclear reactors, the membrane changed its color from blue to pink. The membrane performances were tested by Induced Coupled Plasma–Mass Spectrometry (ICP-MS) analyses showing a separation process efficiency of 86% relative to the initial feed solution.

Keywords: cellulose acetate; surface modification; Gd(III) retention; self-indicating properties

1. Introduction

Gadolinium-based complexes and salts are used for two main applications: as contrast agent components for clinical and research magnetic resonance imaging (MRI) examinations [1,2] and poison for nuclear reactors in order to control the nuclear reaction [3]. The problem of Gd(III) toxicity is given by the fact that traces of this element or other complexes based on Gd(III) can remain in the brain, causing toxic effects [4,5]. Besides the fact that it is a highly toxic element, one of the biggest advantages of using this element in its currently known application is given by the practical situation that it cannot be present in environment, because contrast MRI agents are subject to very strict regulations, and also the water that is used as the nuclear reactors' moderator never goes into the environment due to the same strict regulations. From these reasons, the removal of Gd(III) from water is limited

to the single practical application of regulating the concentration of Gd(III) from the water used to moderate the nuclear reactions. For this application, one single solution is applied: ion exchange resins. Most used resins are based on polystyrene [6], with performances varying from 150 to 178 mg Gd(III)/g of resin. Higher yields for retention can be obtained using mixed bed (MB) resin column consisting of Strong Acid Cation (SAC) resin and Strong Base Anion (SBA) resin [7], achieving a retention of 250 mg Gd(III)/g of resin. New systems based on functionalized mesoporous silica [8,9] or composites with magnetic nanoparticles [10] have been tested, but ion exchange remains the technical solution with the highest retention. Until now, even if we are considering a separation process, no membrane materials have been reported for the removal of Gd(III). We will propose here a revolutionary membrane material that not only has the ability to separate Gd(III) from water used to moderate the nuclear reactions, but also with the remarkable property of changing its color, visually indicating the separation of Gd(III).

Membrane materials are unique among all the materials known and used at this time because, besides their structural and functional characteristics and properties, they possess a unique property: selectivity [11]. A membrane is a functional material that acts essentially as a barrier to a particular species of ions, molecules, and particles, but it is permeable to the rest of the species in a multicomponent system [12]. The development of membrane separation processes was based on both technical factors such as separation selectivity, technology reliability, energy efficiency, and productivity, as well as economic ones such as the cost of plant, equipment [13–15], operating and maintenance [16], and the also price of the raw materials [17]. Membrane and membrane processes constitute an interdisciplinary field whose explosive evolution has been determined by the unlimited involvement of materials science, mathematics, physics, physical chemistry, biology, and engineering in every stage from theory to industrial process. A proof of this is the multiple applications in various fields such as biomedical sciences: hemodialysis [18–20], protein separation [21,22], osteointegration [23–55], fuel cells [26–28], environmental decontamination [29].

After performing a membrane separation process, a very important step is the evaluation of the separation efficiency. For this, different methods of analysis are applied to the solution with separated species, such as UV-Vis spectroscopy [30], atomic abortions [31], and Induced Coupled Plasma–Mass Spectrometry ICP-MS [32].

The present study was conducted for Gd(III) separation from aqueous solutions. Gadolinium nitrate is one of the most used moderators for nuclear reactions which, in the recent year, successfully replaced boron for this type of application [7,33–35]. The basic idea of the current research was to have an easy method to remove gadolinium from aqueous solutions and also the possibility that the membrane would indicate the gadolinium separation without adjacent analysis. Since the solutions used in nuclear power are very pure solutions, the possibility of having other interferences to be separated in the system has been eliminated from the start [36]. The excess of gadolinium must be separated in order to control the nuclear reaction at desired parameters. The underlying principle of this research was to find a substance that simultaneously exhibits two roles: separating the gadolinium from aqueous solutions and to indicate that gadolinium was separated by changing a membrane property that could be slightly observed, changing the color of the membrane surface.

For this purpose, an indicator has been searched that fulfills both conditions and can be immobilized on the membrane surface. Calmagite is an indicator for metal cations with the molecular formula presented in Figure 1. The operating principle of this indicator is based on the complexation reaction of metal cations generated by the two hydroxyl groups and the two nitrogen atoms [37]. The novelty degree of this research is given by the fact that without additional instrumental analysis methods, the efficiency of separation can be observed visibly by the operator through the change of color of the membrane surface.
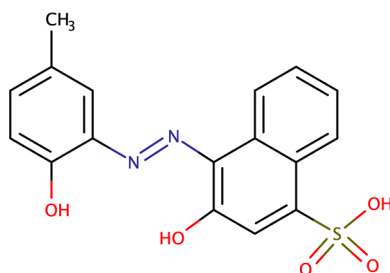
Figure 1. Molecular formula of calmagite.

2. Materials and Methods

In order to functionalize the membrane surface, we have used our previous experience in the modification of the cellulose acetate membranes surface, which implies the following steps: the hydrolysis of acetyl groups to increase the number of hydroxyl groups at the membrane surface, aminopropyl triethoxy silane (APTES) immobilization, and glutaraldehyde (GA) linkages to the amino groups of APTES, followed by immobilization of calmagite. Calmagite immobilization was performed at the –OH group, similar to the resveratrol immobilization previously reported [38]. The immobilization method was originally developed for the immobilization of large molecules such as proteins to improve the response of osteoblasts in the bone regeneration process when metal implants are mounted (the membrane is at the interface between the metallic implant and the bone) [39].

In this study, for the modification of the membrane's surface, asymmetric commercial cellulose acetate (CA) membranes with 0.45 μm porosity on the active surface were used, which were purchased from Lab Box. For the modification of the CA surface with APTES (Sigma Aldrich, St. Louis, MO, USA, analytic reagent) and GA (Merck, Kenilworth, NJ, USA, analytic reagent), our protocol follows the steps previously reported in the literature for sericin and resveratrol immobilization [40,41]. For the partial hydrolysis of the membranes, the membranes were treated with a sodium hydroxide solution, the APTES immobilization reaction being carried out in a weak basic catalysis using a 0.1 N sodium hydroxide solution. After the reaction, the membranes were washed with deionized water for removing unreacted APTES. For the immobilization of calmagite (Sigma Aldrich, analytical purity), glutaraldehyde was used as a linker molecule between APTES and calmagite. After the reaction has been completed, the membranes are washed and stored in cold, ultra-pure water to avoid the formation and proliferation of microorganisms on the surface.

The synthesized membranes were analyzed by infrared spectroscopy with Fourier transform FT-IR using a Bruker Vertex 70 (Bruker, Billerica, MA, USA) equipment with a diamond ATR device in the range of 600–4000 cm^{-1}. The spectra were recorded as an average of 32 successive measurements, eliminating bands of noise, atmospheric CO_2, and atmospheric water vapor. Raman spectra were registered on a DXR Raman Microscope from Thermo Scientific (Thermo Fischer, Waltham, MA, USA) using a 633 nm laser line and a number of 10 scans. The laser beam was focused with a 10X objective of the Raman microscope.

Thermal analysis (TGA) curves were registered on Q500 TA Instruments equipment (TA Instruments, New Castle, DE, USA), using nitrogen atmosphere from room temperature to 700 °C and a heating rate of 10 °C/min.

The surface structures for CA and modified CA were studied by X-ray photoelectron spectroscopy (XPS) using a K-Alpha instrument from Thermo Scientific (Thermo Fischer, Waltham, MA, USA), with a monochromated Al Kα source (1486.6 eV), at a bass pressure of 2×10^{-9} mbar. The absolute calibration of the binding energy scale was performed using Au 4f$_{7/2}$ (reference binding energy 83.96 eV), Ag 3d$_{5/2}$ (reference binding energy 368.21 eV), Cu 2p$_{3/2}$ (reference binding energy 932.62 eV). The pass energy for the survey spectra was 200 eV [41–43]. The fastest scan rate for survey spectra was 1 eV, and the lowest for high-resolution spectra was 0.1 eV.

The morphological characterization of the pure CA and functionalized CA membranes was made using a Philips XL 30 ESEM TMP scanning electron microscopy (SEM) (FEI/Philips, Hillsboro, OR, USA).

The flows were measured on a Sartorius module, using 47 mm filtering membranes and 250 mL of distilled water.

The water flux (*Wf*) expressed in $L \cdot m^{-2} \cdot h^{-1}$ was calculated by the following formula (Equation (1)):

$$Wf = \frac{V}{A \cdot t} \tag{1}$$

where *Wf* is the water flux, *V* is the volume (L) of the feed solution, *A* is the area (m^2) of the membrane, and *t* is the time (h).

Gadolinium retention was studied using a gadolinium nitrate feed solution in ultrapure water (1 g/L), the analysis being performed on the filtered solutions using the ICP-MS technique, using a Bruker Instrument (Bruker, Billerica, MA, USA). Retention was calculated using the following formula:

$$R = 100 - \frac{C_F}{C_P} * 100 \tag{2}$$

where *R* is the Gd(III) retention (%), and C_F and C_P are the concentrations ($g \cdot L^{-1}$) of Gd(III) in the feed and the permeate, respectively.

3. Results

SEM microscopy (Figure 2) revealed some important aspects regarding the morphological changes of synthesized membranes surface. Unlike cellulose acetate standard membrane, the APTES functionalized membrane presents a low surface porosity due to the cross-linking effect induced by covalent interaction between APTES and free hydroxyl groups at the membrane surface. In addition, in the case of an APTES functionalized membrane, on the porous surface, a series of agglomerations are observed due to the APTES polymerization in the presence of traces of water in the alcohol during the functionalization reaction.

As a result of the calmagite immobilization, the surface fiber structure increases greatly, which is most probably due to the rejection of calmagite molecules (a large number of uninvolved electrons in nitrogen atoms and oxygen atoms from sulfonic acid groups). After gadolinium filtering, the surface morphology changes in the fibers approaching direction. This is due to the complexation reaction that takes place between the non-participating electrons from the nitrogen atoms and the hydroxyl groups in the adjacent molecules, which also results in a cross-linking and tightening of the surface. Moreover, on the porous surface, we can observe the presence of large crystals of gadolinium, which probably formed around growth sites that were born in the initial calmagite complexation.

As can be seen from Figure 2, the optical aspect of the synthesized membranes revealed that the basic principle from which the idea of this research started works. In the membrane functionalization phases of hydrolysis—the immobilization of APTES and glutaraldehyde—the surface of the membrane remains white. After calmagite immobilization, the surface of the membrane can be seen in a dark blue color. After the filtration of gadolinium nitrate, a radical change in color from dark blue to pink can be seen, which is visible to the naked eye; besides the separating properties, the membrane also exhibit self-indicating properties.
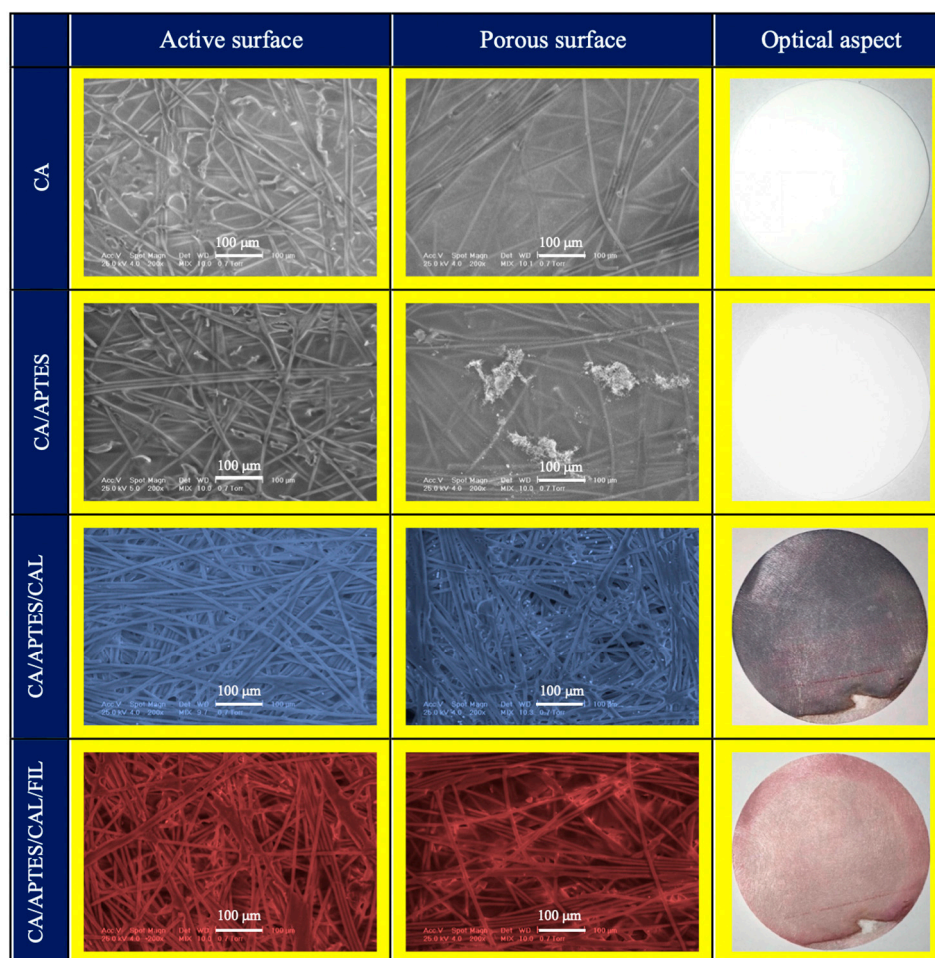
Figure 2. Scanning Electron Microscopy of synthesized membranes (active surface and porous surface) and optical aspect with evolution of color changing on the surface from dark blue for functionalized membrane with calmagite (CA/APTES/CAL) before and after filtration of Gd(III) to pink (CA/APTES/CAL/FIL) where FIL—filtration. APTES: Aminopropyl triethoxy silane, CA: Cellulose acetate.

FT-IR spectra (Figure 3) exhibit major changes, proving the functionalization of the used membranes. Thus, after the partial hydrolysis of cellulose acetate membranes, in order to increase the number of hydroxyl groups at the surface of the membrane, the band specific for C=O decreases in intensity because the number of acetyl groups have been reduced during the hydrolysis process. In addition, functionalization with APTES causes a movement of all of the bands due to the presence of Si atoms. The immobilization of calmagite caused an intensity modification of all bands (due to functional groups changes in relation to the total membrane surface: the presence of –N=N– and –SO_3H), as well as their slight displacement (for the same reasons). The 1750 cm^{-1} band, assigned to C=O groups, has the highest intensity in cellulose acetate, which is highly diminished after hydrolysis with sodium hydroxide. The band is still present in the case of other membranes, which indicates that the hydrolysis of the membrane is not complete, leaving fewer C=O groups behind. In addition, another decrease in intensity can be observed for the 1250 cm^{-1} band assigned to the etheric groups C–O. This is also explained by the partial hydrolysis of acetyl groups in cellulose acetate, but it can also be due to the hydrolysis of the polymer chains, as indicated by the thermal analysis. However, the formation of new ether connections also occurs by immobilizing APTES on the surface of the membrane. The decreased intensity of the band can be explained by breaking the multiple bindings rather than forming new bindings, as well as by steric hindrance generated by APTES's high molecular volume. Other changes occur in the 3200–3600 cm^{-1} region that are specific for hydrogen bonding in

water and hydroxyl groups. In the case of cellulose acetate after treatment with sodium hydroxide (to increase the number of –OH groups), band intensity increases due to the increase in hydroxyl groups number. Intensity is also very high for the CA/APTES/GA membrane because of the cross-linking effect on the membrane and high water retention [44–47].
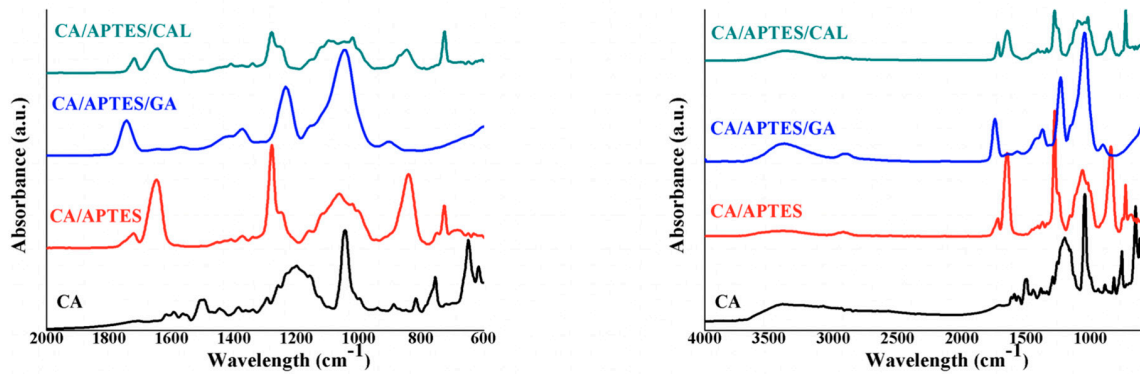

Figure 3. Fourier transform infrared spectroscopy (FT-IR) spectra of synthesized CA, CA/APTES, CA/APTES/GA, and CA/APTES/CAL membranes with details for the range 600–2000 cm^{-1} (**left**) and 500–4000 cm^{-1} (**right**). GA: Glutaraldehyde.

Calmagite immobilization on the functionalized membrane surface can be observed in the IR spectrum of the CA/APTES/GA/CAL membrane where, besides the cellulose acetate corresponding bands, one can notice the presence of two additional bands at 1579 and 1520 cm^{-1} from the CAL structure. These peaks correspond to the stretching vibration of the C=O and NH$_2$ amide bonds and are consistent with the values reported in the literature [48].

These results were further supported by their respective Raman spectra (Figure 4). Several new peaks attributed to the presence of new functional groups on the pristine membrane were clearly visible. The intensities of the pristine membrane peaks were higher after functionalization, resulting in an enhanced surface showed by resonance scattering [40].
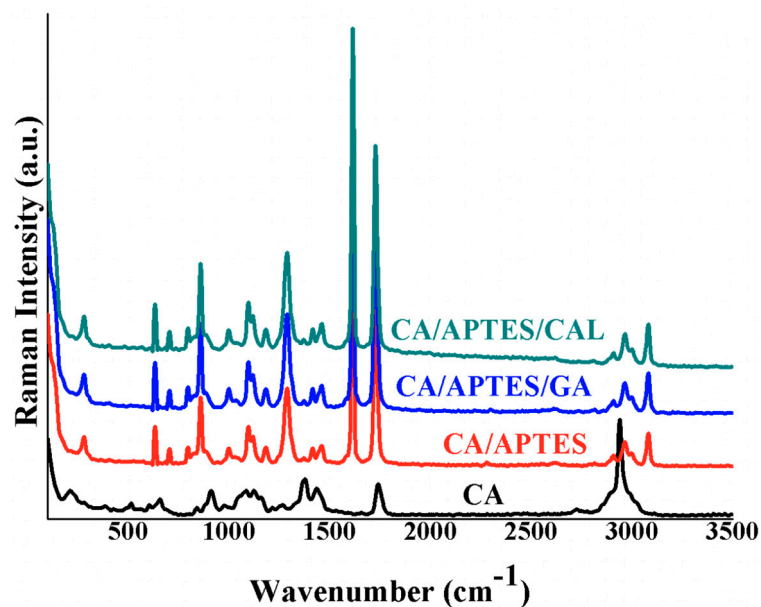

Figure 4. Raman spectra of synthesized CA, CA/APTES, CA/APTES/GA, and CA/APTES/CAL membranes.

　　　More proof that the functionalization process takes place is shown in the XPS survey curves depicted in Figure 5. The XPS analysis was performed in order to observe the modification of the chemical composition of CA surface after the functionalization process. The XPS survey spectrum of CA exhibits two peaks assigned to C 1s and O 1s located at 284.72 eV and 531.34 eV, respectively. The functionalization of the CA membrane's surface leads to some changes both in the atomic percent of C 1s and O 1s and also to the appearance of some new peaks in the XPS survey spectra. For example, in the XPS survey spectra of CA/APTES, the percent of C 1s increases from 45.16% to 64.96% and the O 1s percent decreases from 44.8% to 20.49%. In addition, beside the CA peak, a new peak located at 102.12 eV assigned to Si 2p (8.64%) could be observed and this indicates that the linking of APTES to the membrane surface. The further functionalization step involves the reaction with GA, which exhibits the following atomic percent: 62.69% for C 1s, 28.64% for O 1s, 5.34% for N 1s, and 3.7% Si 2p. The immobilization of calmagite is demonstrated by an increase of O 1s percent to 25.04% and a decrease of C 1s atomic percent to 63.27%, and this is due to the orientation of the calmagite molecules at the surface, which can be recorded by XPS equipment. In addition, the N 1s atomic percent decrease to 3.24% is due to the shield of the steric planarity induced by the polarity of the aromatic naphthalene rings. The XPS results prove that the modification process was achieved.

　　　In order to prove the functionalization of CA, the C 1s (Figure 6), O 1s (Figure 7), N 1s, and Si 2p (Figure 8) high-resolution spectra were recorded for the samples. According to Figure 6, after the APTES functionalization, a peak at 281 eV appears, which is attributed to C-Si. In addition, in the CA/APTES sample, the peak at 288 eV is attributed to a C–N bond. The intensity of the O–C–O peak (at a binding energy of 289 eV) is increased in the case of CA/APTES sample due to the increase of these bonds after the immobilization of APTES. The next step of functionalization (reaction with GA) was demonstrated by the presence of a new peak at 288 eV, which is assigned to C=N [49–51].

　　　In addition, O 1s spectrum (Figure 7) can be deconvoluted to three peaks centered at 530, 531, and 532 assigned to O=C, O–C, and O–H for the CA sample, respectively. In the case of CA/APTES, the appearance of an O–Si specific peak at 529 eV suggests the immobilization at the surface of the membrane of APTES. After the immobilization of calmagite, O=S at 534 eV, this bond being present only in the structure of the used indicator [49–51].
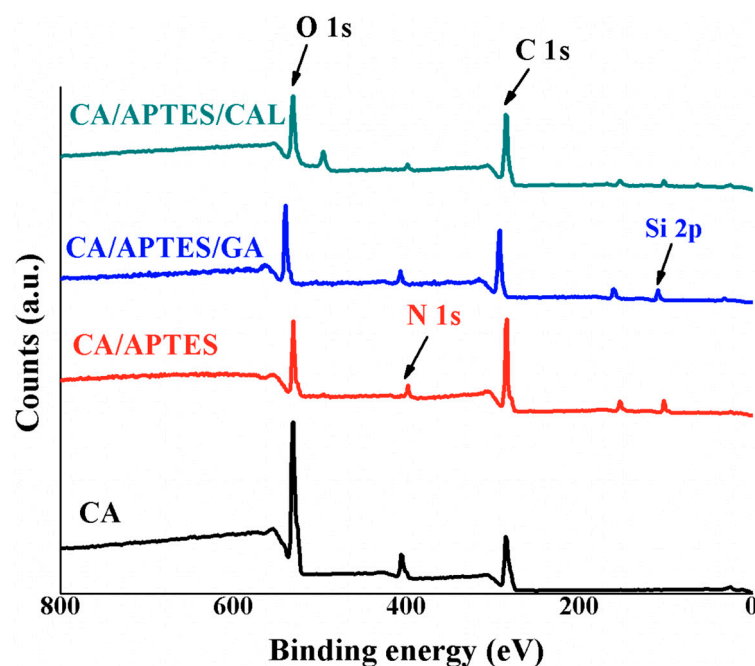

Figure 5. X-ray photoelectron spectroscopy (XPS) survey analysis of CA, CA/APTES, CA/APTES/GA, and CA/APTES/CAL membranes with marked interest peaks for C 1s, O 1s, Si 2p, and N 1s.
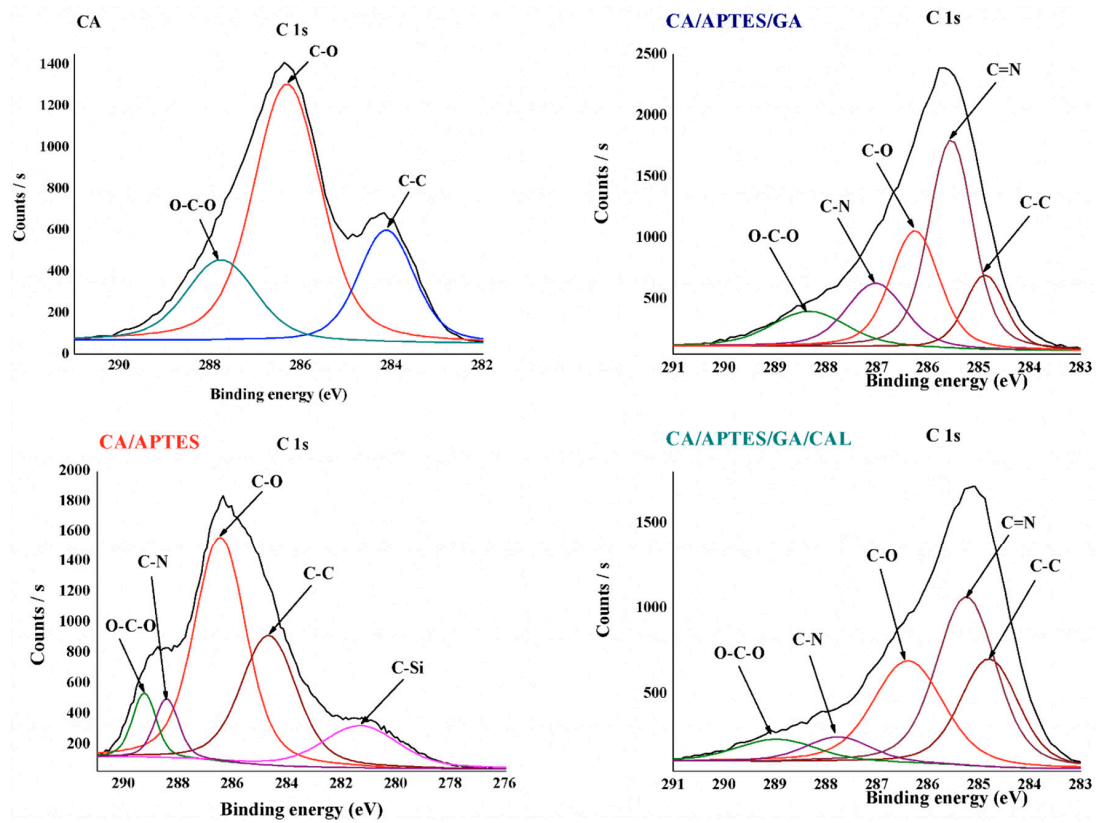
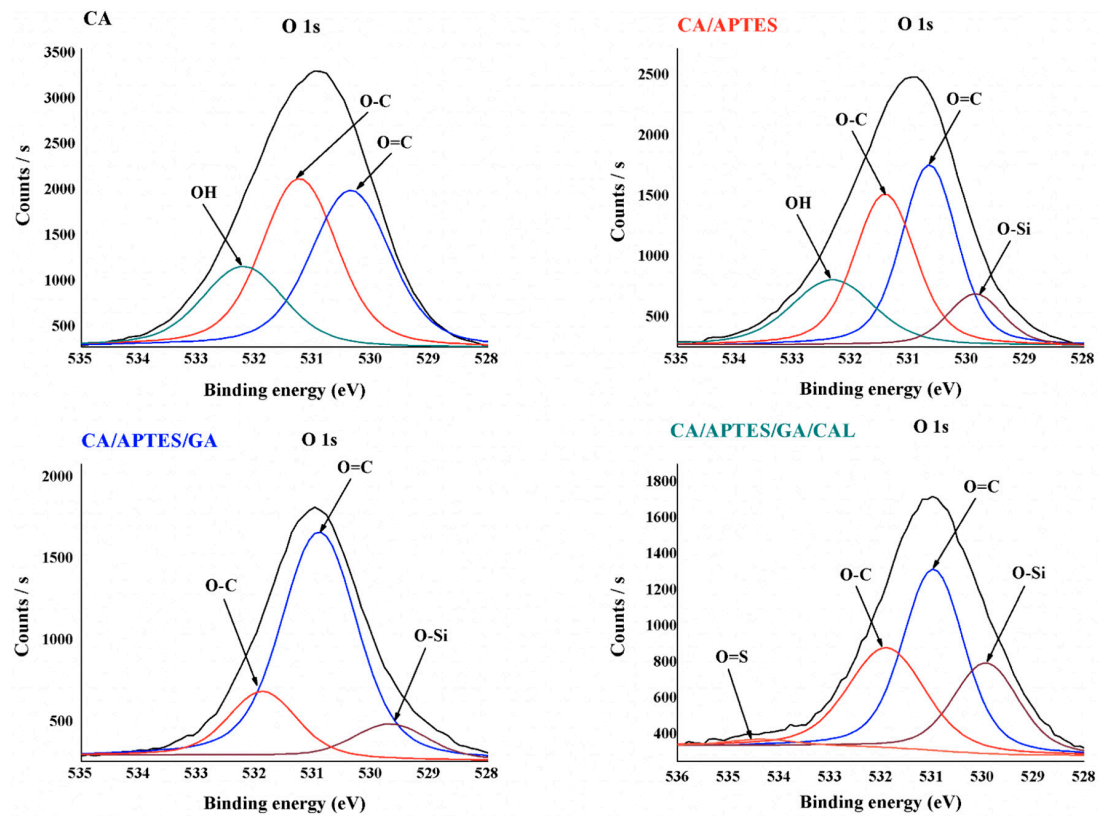**Figure 6.** The fitted C 1s spectra for synthesized samples.

Figure 7. The fitted O 1s spectra for synthesized samples.

In Figure 8, deconvoluted spectra for N 1s show the presence of N–C bonds in CA/APTES, CA/APTES/GA, respectively CA/APTES/GA/CAL, at 399 eV and N=C bonds in CA/APTES/GA and CA/APTES/GA/CAL samples, at 402 eV [52]. Related to deconvoluted spectra for Si 2p, we can observe Si–O (at 103 eV) and Si–C bonds (at 102 eV) from APTES used as linkers and present in CA/APTES, CA/APTES/GA, and CA/APTES/GA/CAL samples [53].
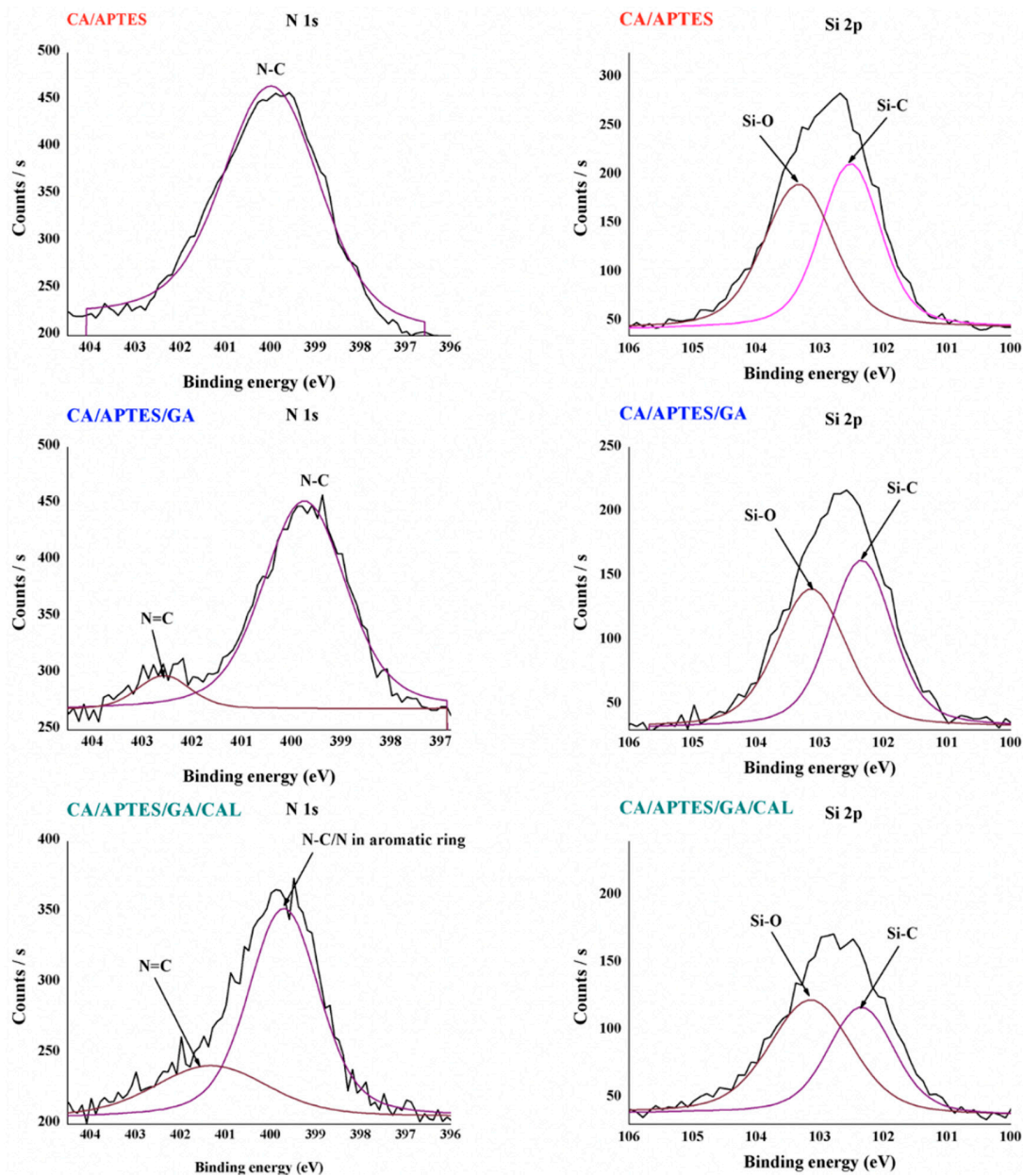
Figure 8. The fitted N 1s and Si 2p spectra for synthesized samples.

For industrial applications, the thermal stability of the material is also an important parameter. Considering this, the thermal stability and the degradation profile of the pure CA and modified CA membranes were assessed by thermal analysis (Figure 9). The pure CA membranes show the typical decomposition profile with two degradation steps attributed to the evaporation of the solvent and to the degradation of the CA polymer chain [30]. In the case of the modified CA membranes, the thermal degradation profiles illustrate a similar trend as for the pure CA membrane, which means that the synthesized materials are thermally stable. Figure 9 show an increase of the residual mass in the case

of the CA/APTES membrane, which could be attributed to the SiO$_2$ moieties from APTES structure and might prove that the immobilization of the silane-coupling agent on the CA surface was achieved [54].

The lowest residual mass (2%) was registered in the case of the CA/APTES/GA/CAL and is due to the thermal degradation of the organic moistures attached on the CA membrane's surface. There are many studies that demonstrate that the degradation temperature depends on the functional groups grafted on the cellulose acetate surface [55].
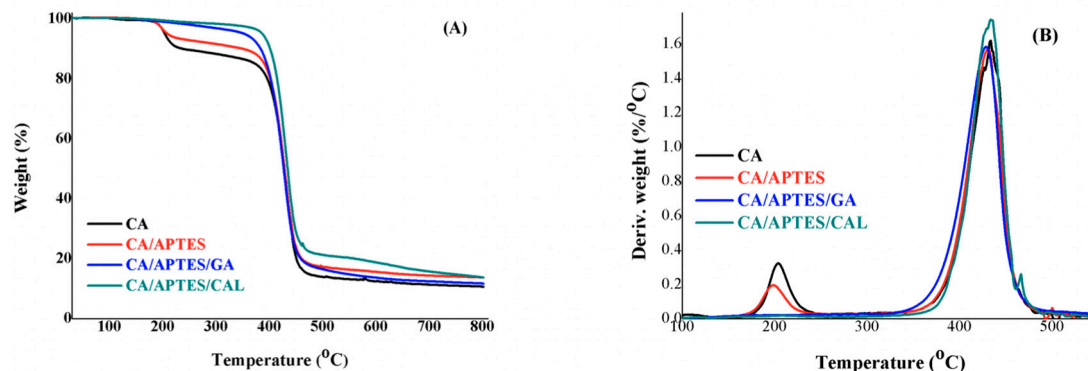

Figure 9. TGA (**A**)– Differential Thermal Analysis DTA (**B**) spectra of CA, CA/APTES, CA/APTES/GA, and CA/APTES/CAL membranes.

The temperature at which the mass loss is 5% (Td$_{5\%}$) was recorded in order to show the thermal stability of the as-synthesized membrane. The data reported in the Table 1 indicate a significant increase of the thermal stability of the modified CA membrane after each modification step. The enhancement of the thermal stability of the CA/APTES membrane is assigned to the chemical interaction between the hydroxyl groups from CA and APTES. Moreover, this increase of the thermal stability could be a consequence of the slight cross-linking effect induced after immobilization of APTES onto the CA surface supported also by SEM images [56]. In the case of CA/APTES/GA, the enhancement of the thermal stability corresponds to the strong interlinks obtained in the CA/APTES/GA membrane, as has been noticed in our previous studies [41]. The highest thermal stability was registered in the case of the membrane with calmagite immobilized on the CA surface. This could be mainly assigned to the highly thermal stable naphthalene rings and strong interlinks built on the cellulose acetate surface. Similar behavior was also observed by Abdel-Naby et al. when they succeeded in chemically modifying cellulose acetate with diallylamine [57]. The Derivative Thermogravimetry DTG results show no significant changes.

Table 1. The wt (%), Td$_{5\%}$ and the DTG values for the CA membrane before and after the modification process. Three different samples were analyzed for calculating the standard deviation.

Sample Name	wt (%)	Td$_{5\%}$ (°C)	DTG (°C)
CA	89 ± 1	204 ± 3	433 ± 1
CA/APTES	86 ± 1	281 ± 3	431 ± 1
CA/APTES/GA	88 ± 1	352 ± 3	430 ± 1
CA/APTES/GA/CAL	98 ± 1	372 ± 3	433 ± 1

The thermal behavior of the membrane is not radically modified, indicating the stability of the synthesized during the transformation process. The small changes can be explained by multiple chemical modifications of the synthesized membranes, which have an effect not only on the immobilization of calmagite, but also on the partial hydrolysis of the polymer that constitutes the material. The highest thermal stability in the case of CA/APTES/GA/CAL is attributed to the presence of covalent bonds in the entire structure of the material.

Flows through synthesized membranes (Figure 10) were also studied, and membrane retention capacity was evaluated by five successive passes of 500 mL of 1 g/L aqueous solution of gadolinium

nitrate. In the case of neat cellulose acetate membrane, initial water flow was about 160 L/m^{2}h, but after functionalization with calmagite, the flow increased to approximately 600 L/m^{2}h. This can be explained by the hydrophilicity of calmagite molecule, which also induces a higher hydrophilic character to the membrane material. After the first recirculation cycle, the decrease of flow can be explained by the hydrodynamic stabilization of polymer layers inside the membrane structure.

Total retention (Figure 11), assessed by ICP-MS, was 86% for the functionalized membrane, compared to 64% for the cellulose acetate standard membrane. This difference can be explained by the complexation reaction of calmagite indicator immobilized at the surface of the membrane. In addition, consequently with higher values of retention, the change in surface color occurs, visually indicating the retention of Gd(III). Further studies related to this new generation of membrane materials will envisage and validate calibration methods for visually indicating the concentration of retained cation depending on the color of the surface.
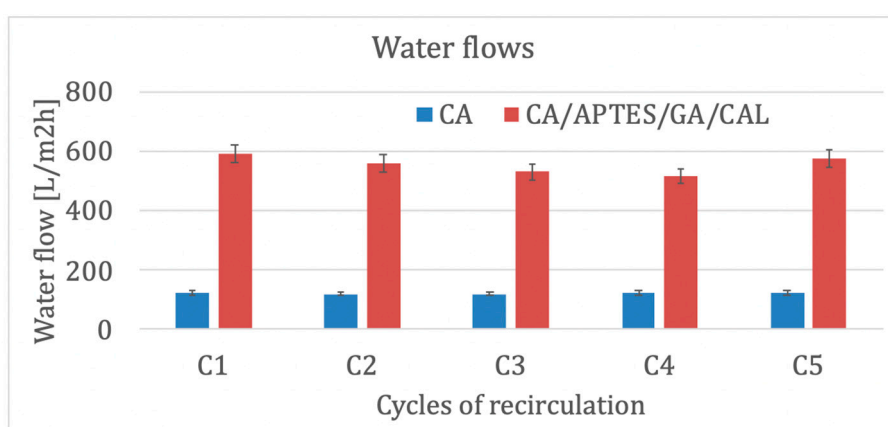

Figure 10. Water flows through CA and CA/APTES/GA/CAL membranes. Five different measurements for calculating standard error.
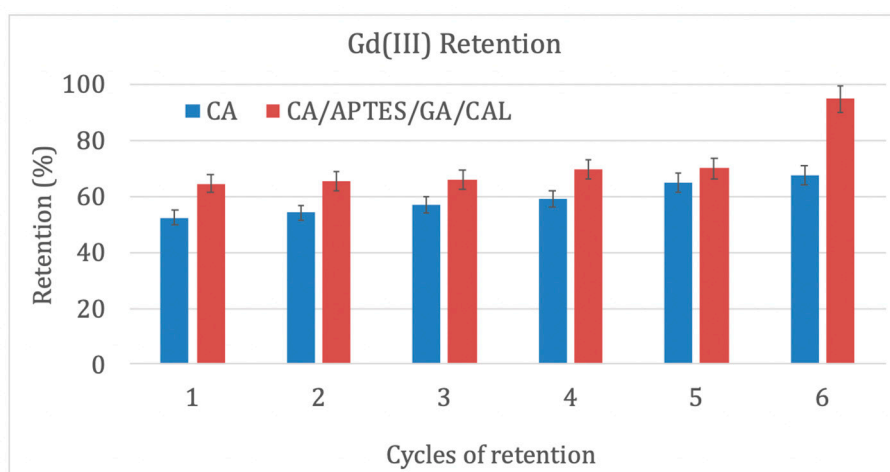

Figure 11. Gd(III) retention (%) related to feed solution through CA and CA/APTES/GA/CAL membranes. Five different measurements for calculating standard error.

4. Conclusions

A new, revolutionary, and easy method for evaluating the separation process through a membrane was presented, based on the fact that each separated chemical compound will react with an immobilized indicator at the surface of the membrane, which will change the surface color of the membrane.

Calmagite was chosen for its dual role as a molecule that will complex and retain Gd(III) and also as an indicator for Gd(III). At the contact with the membrane surface, calmagite will actively complex and retain Gd(III), and it will change the color of the membrane surface during the complexation process, showing that the separation occurred. This was achieved by the functionalization of a cellulose acetate polymeric membrane in three steps, with amino propyl triethoxysilane, glutaraldehid, e and calmagite. The synthesized membranes showed good thermal stability (due to the multiple functionalization steps (which induces a cross-linking effect to the entire material). In addition, synthesized membranes were characterized by FT-IR, Raman, and XPS in order to prove the functionalization reactions. Moreover, in the separation of the Gd(III) process, having gadolinium nitrate as a source that was used as a moderator in nuclear reactors, the membrane changed its color from blue to pink, and ICP-MS analyses showed a separation process efficiency of 86% relative to the initial feed solution after 5 cycles of recirculation.

References

1. Costa, A.F.; Van Der Pol, C.B.; Maralani, P.J.; McInnes, M.D.; Shewchuk, J.R.; Verma, R.; Hurrell, C.; Schieda, N. Gadolinium deposition in the brain: A systematic review of existing guidelines and policy statement issued by the canadian association of radiologists. *Can. Assoc. Radiol. J.* **2018**, *69*, 373–382. [CrossRef] [PubMed]

2. Abujudeh, H.H.; Kosaraju, V.K.; Kaewlai, R. Acute adverse reactions to gadopentetate dimeglumine and gadobenate dimeglumine: Experience with 32,659 injections. *Am. J. Roentgenol.* **2010**, *194*, 430–434. [CrossRef] [PubMed]

3. Dalle, H.M.; de Mattos, J.R.L.; Dias, M.S. Enriched gadolinium burnable poison for PWR fuel – Monte carlo burnup simulations of reactivity, chapter-4. In *Current Research in Nuclear Reactor Technology in Brazil and Worldwide*; Intech Publishers: Rijeka, Croatia, 2013; pp. 73–89.

4. Kanda, T.; Fukusato, T.; Matsuda, M.; Toyoda, K.; Oba, H.; Kotoku, J.; Haruyama, T.; Kitajima, K.; Furui, S. Gadolinium-based contrast agent accumulates in the brain even in subjects without severe renal dysfunction: Evaluation of autopsy brain specimens with inductively coupled plasma mass spectroscopy. *Radiolgy* **2015**, *276*, 228–232. [CrossRef] [PubMed]

5. Murata, N.; Gonzalez-Cuyar, L.F.; Murata, K. Macrocyclic and other non-group 1 gadolinium contrast agents deposit low levels of gado- linium in brain and bone tissue: Preliminary results from 9 patients with normal renal function. *Investig. Radiol.* **2016**, *51*, 447–453. [CrossRef]

6. Elsofany, E. Removal of lanthanum and gadolinium from nitrate medium using Aliquat-336 impregnated onto Amberlite XAD-4. *J. Hazard. Mater.* **2008**, *153*, 948–954. [CrossRef]

7. Rufus, A.; Kumar, P.S.; Jeena, K.; Velmurugan, S. Removal of gadolinium, a neutron poison from the moderator system of nuclear reactors. *J. Hazard. Mater.* **2018**, *342*, 77–84. [CrossRef]

8. Tadjarodi, A.; Jalalat, V.; Zare-Dorabei, R. Adsorption of La(III) in aqueous systems by N-(2-hydroxyethyl) salicylaldimine-functionalized mesoporous silica. *Mater. Res. Bull.* **2015**, *61*, 113–119. [CrossRef]

9. Zare-Dorabei, R.; Jalalat, V.; Tadjarodi, A. Central composite design optimization of Ce(iii) ion removal from aqueous solution using modified SBA-15 mesoporous silica. *New J. Chem.* **2016**, *40*, 5128–5134. [CrossRef]

10. Dashtian, K.; Zare-Dorabei, R. Synthesis and characterization of functionalized mesoprous SBA-15 decorated with Fe_3O_4 nanoparticles for removal of Ce(III) ions from aqueous solution: ICP–OES detection and central composite design optimization. *J. Colloid Interface Sci.* **2017**, *494*, 114–123. [CrossRef]

11. Ulbricht, M. Advanced functional polymeric membranes. *Polymer* **2006**, *47*, 2217–2262. [CrossRef]

12. Thakur, V.; Voicu, S.I. Recent advances in cellulose and chitosan based membranes for water purification: A concise review. *Carbohydr. Polym.* **2016**, *146*, 148–165. [CrossRef] [PubMed]

13. Anitha, A.; Sowmya, S.; Jayakumar, R.; Deepthi, S.; Chennazhi, K.; Ehrlich, H.; Tsurkan, M.; Jayakumar, R. Chitin and chitosan in selected biomedical applications. *Prog. Polym. Sci.* **2014**, *39*, 1644–1667. [CrossRef]

14. Corobea, M.; Muhulet, O.; Miculescu, F.; Antoniac, I.V.; Vuluga, Z.; Florea, D.; Vuluga, D.M.; Butnaru, M.; Ivanov, D.; Voicu, S.I.; et al. Novel nanocomposite membranes from cellulose acetate and clay-silica nanowires. *Polym. Adv. Technol.* **2016**, *27*, 1586–1595. [CrossRef]

15. Corobea, C.; Donescu, D.; Rădiţoiu, S.; Voicu, S.I.; Nechifor, G. Membrane materials IV. Functionalised hybrid polimer nanoparticles for copper ions separation on colloidal ultrafiltration. *Revista de Chimie.* **2006**, *57*, 981–987.

16. Thakur, V.; Thakur, M.K. Processing and characterization of natural cellulose fibers/thermoset polymer composites. *Carbohydr. Polym.* **2014**, *109*, 102–117. [CrossRef]

17. Thakur, V.; Thakur, M.K.; Gupta, R.K. Rapid synthesis of graft copolymers from natural cellulose fibers. *Carbohydr. Polym.* **2013**, *98*, 820–828. [CrossRef]

18. Voicu, S.I.; Dobrica, A.; Sava, S.; Ivan, A.; Naftanaila, L. Cationic surfactants-controlled geometry and dimensions of polymeric membrane pores. *J. Optoelectron. Adv. Mater.* **2012**, *14*, 923–928.

19. Voicu, S.I.; Ninciuleanu, C.M.; Muhulet, O.; Miculescu, M. Cellulose acetate membranes with controlled porosity and their use for the separation of aminoacids and proteins. *J. Optoelectron. Adv. Mater.* **2014**, *16*, 903–908.

20. Rusen, E.; Mocanu, A.; Nistor, L.C.; Dinescu, A.; Călinescu, I.; Mustăţea, G.; Voicu, Ş.I.; Andronescu, C.; Diacon, A. New design of antimicrobial membranes based on polymers colloids/MWCNT hybrid materials and silver nanoparticles. *ACS. Appl. Mater. Interfaces* **2014**, *6*, 17384–17393. [CrossRef]

21. Miculescu, M.; Muhulet, A.; Nedelcu, A.; Voicu, S.I. Synthesis and characterization of polysulfone - carbon nanotubes - polyethylene imine composite membranes. *Optoelectron. Adv. Mater.* **2014**, *8*, 1072–1076.

22. Dumitriu, C.; Voicu, S.I.; Muhulet, A.; Nechifor, G.; Popescu, S.; Ungureanu, C.; Carja, A.; Miculescu, F.; Trusca, R.; Pirvu, C. Cellulose acetate - titanium dioxide nanotubes membrane fraxiparinized through polydopamine. *Carbohydr. Polym.* **2018**, *181*, 215–223. [CrossRef] [PubMed]

23. Miculescu, F.; Maidaniuc, A.; Voicu, S.I.; Thakur, V.; Stan, G.; Ciocan, L.T. Progress in hydroxyapatite–starch based sustainable biomaterials for biomedical bone substitution applications. *ACS Sustain. Chem. Eng.* **2017**, *5*, 8491–8512. [CrossRef]

24. Miculescu, F.; Mocanu, A.C.; Stan, G.; Miculescu, M.; Maidaniuc, A.; Cimpean, A.; Mitran, V.; Voicu, S.I.; Machedon-Pisu, T.; Ciocan, L.T. Influence of the modulated two-step synthesis of biogenic hydroxyapatite on biomimetic products' surface. *Appl. Surf. Sci.* **2018**, *438*, 147–157. [CrossRef]

25. Maidaniuc, A.; Miculescu, F.; Andronescu, C.; Miculescu, M.; Matei, E.; Pencea, I.; Csaki, I.; Machedon-Pisu, T.; Ciocan, L.T.; Voicu, S.I.; et al. Induced wettability and surface-volume correlation of composition for bovine bone derived hydroxyapatite particles. *Appl. Surf. Sci.* **2018**, *438*, 158–166. [CrossRef]

26. Muhulet, A.; Miculescu, F.; Voicu, S.I.; Schütt, F.; Thakur, V.; Mishra, Y.K. Fundamentals and scopes of doped carbon nanotubes towards energy and biosensing applications. *Mater. Today Energy* **2018**, *9*, 154–186. [CrossRef]

27. Bresciani, R.; Marzorati, S.; Lascialfari, A.; Sacchi, B.; Santo, N.; Longhi, M. Effects of catalyst aging on the growth morphology and oxygen reduction activity of nitrogen-doped carbon nanotubes. *Electrochem. Commun.* **2015**, *51*, 27–32. [CrossRef]

28. Yu, L.-H.; Wang, R.; Xu, L. Preparation of acylamino copper Phthalocyanine modified multiwalled carbon nanotubes thin films with oxygen plasma treatment. *Mater. Lett.* **2016**, *164*, 282–285. [CrossRef]

29. Ioniţă, M.; Crica, L.E.; Voicu, S.I.; Dinescu, S.; Miculescu, F.; Costache, M.; Iovu, H. Synergistic effect of carbon nanotubes and graphene for high performance cellulose acetate membranes in biomedical applications. *Carbohydr. Polym.* **2018**, *183*, 50–61. [CrossRef]

30. Raicopol, M.D.; Andronescu, C.; Voicu, S.I.; Vasile, E.; Pandele, A.M. Cellulose acetate/layered double hydroxide adsorptive membranes for efficient removal of pharmaceutical environmental contaminants. *Carbohydr. Polym.* **2019**, *214*, 204–212. [CrossRef]

31. Shin, Y.; Taufique, M.F.N.; Devanathan, R.; Cutsforth, E.C.; Lee, J.; Liu, W.; Fifield, L.S.; Gotthold, D. Highly selective supported graphene oxide membranes for water-ethanol separation. *Sci. Rep.* **2019**, *9*, 2251. [CrossRef]

32. Mahmoudi, E.; Ng, L.Y.; Ang, W.L.; Chung, Y.T.; Rohani, R.; Mohammad, A.W. Enhancing morphology and separation performance of polyamide 6,6 membranes by minimal incorporation of silver decorated graphene oxide nanoparticles. *Sci. Rep.* **2019**, *9*, 1216. [CrossRef] [PubMed]

33. Mal, D.; Puspalata, R.; Rangarajan, S.; Velmurugan, S. Effect of gadolinium nitrate concentration on molecular product yield during gamma irradiation and on corrosion of stainless steel. *Radiat. Phys. Chem.* **2017**, *138*, 1–8. [CrossRef]

34. Tonoike, K.; Miyoshi, Y.; Uchiyama, G. Benchmark critical experiments of a heterogeneous system of uranium fuel rods and uranium solution poisoned with gadolinium, and application of their results to JACS validation. *J. Nucl. Sci. Technol.* **2011**, *48*, 1118–1128. [CrossRef]

35. Smolen, G.R.; Lloyd, R.C.; Matsumoto, T. Criticality data and validation studies of mixed-oxide fuel pin arrays in Pu+U+Gd nitrate. *Nucl. Technol.* **1994**, *107*, 340–355. [CrossRef]

36. Bierman, S.R. Reactivity measurements under conditions typical to fuel element dissolution. *Nucl. Technol.* **1976**, *31*, 339–347. [CrossRef]

37. Soury, R.; Jabli, M.; Saleh, T.A.; Kechich, A.; Loiseau, F.; Saint-Aman, E.; Nasri, H. Degradation of calmagite by dichloride (5,10,15,20 tetraphenylporphyrinato) antimony hexachloridoantimonate: [Sb(TPP)Cl$_2$]SbCl$_6$. *Inorg. Chem. Commun.* **2019**, *104*, 54–60. [CrossRef]

38. Pandele, A.M.; Neacsu, P.; Cimpean, A.; Staras, A.; Miculescu, M.; Iordache, A.; Voicu, S.; Thakur, V.; Toader, O. Cellulose acetate membranes functionalized with resveratrol by covalent immobilization for improved osseointegration. *Appl. Surf. Sci.* **2018**, *438*, 2–13. [CrossRef]

39. Pandele, A.M.; Comanici, F.; Carp, C.; Miculescu, M.; Voicu, S.; Thakur, V.; Serban, B. Synthesis and characterization of cellulose acetate-hydroxyapatite micro and nano composites membranes for water purification and biomedical applications. *Vacuum* **2017**, *146*, 599–605. [CrossRef]

40. Voicu, S.I.; Condruz, R.M.; Mitran, V.; Cimpean, A.; Miculescu, F.; Andronescu, C.; Miculescu, M.; Thakur, V.K. Sericin covalent immobilization onto cellulose acetate membranes. *ACS Sustain. Chem. Eng.* **2016**, *4*, 1765–1774. [CrossRef]

41. Greczynski, G.; Hultman, L. X-ray photoelectron spectroscopy: Towards reliable binding energy referencing. *Prog. Mater. Sci.* **2020**, *107*, 100591. [CrossRef]

42. Greczynski, G.; Hultman, L. Compromising science by ignorant instrument calibration-need to revisit half a century of published XPS data. *Angew. Chem. Int. Ed.* **2020**, *59*, 5002–5006. [CrossRef] [PubMed]

43. ISO. *15472:2010 Surface Chemical Analysis—X-ray Photoelectron Spectrometers—Calibration of Energy Scales*; ISO: Geneva, Switzerland, 2010.

44. Corobea, M.S.; Albu, M.G.; Ion, R.; Cimpean, A.; Miculescu, F.; Antoniac, I.V.; Raditoiu, V.; Sirbu, I.; Stoenescu, M.; Voicu, S.I.; et al. Advanced modification of titanium surface with collagen and doxycycline, a new approach in dental implants. *J. Adh. Sci. Technol.* **2015**, *29*, 2537–2550. [CrossRef]

45. Ionită, M.; Pandele, A.M.; Crica, L.E.; Voicu, S.I.; Iovu, H. Fabrication of cellulose triacetate/graphene oxide porous membrane. *Polym. Adv. Technol.* **2015**, *27*, 350–357. [CrossRef]

46. Hu, B.-B.; Wang, J.-L.; Wang, Y.-T.; Zhu, M.-J. Specify the individual and synergistic effects of lignocellulose-derived inhibitors on biohydrogen production and inhibitory mechanism research. *Renew. Energy* **2019**, *140*, 397–406. [CrossRef]

47. Gao, X.; Xu, Y.; Ma, M.; Rao, K.; Wang, Z. Simultaneous passive sampling of hydrophilic and hydrophobic emerging organic contaminants in water. *Ecotoxicol. Environ. Saf.* **2019**, *178*, 25–32. [CrossRef]

48. Wasim, M.; Sabir, A.; Shafiq, M.; Khan, R.U. Fractionation of direct dyes using modified vapor grown carbon nanofibers and zirconia in cellulose acetate blend membranes. *Sci. Total. Environ.* **2019**, *677*, 194–204. [CrossRef]

49. Cazzola, M.; Corazzari, I.; Prenesti, E.; Bertonea, E.; Vernè, E.; Ferraris, S. Bioactive glass coupling with natural polyphenols: Surfacemodification, bioactivity and anti-oxidant ability. *Appl. Surf. Sci.* **2016**, *367*, 237–248. [CrossRef]

50. Zhang, X.; Ferraris, S.; Prenesti, E.; Verné, E. Surface functionalization of bioactive glasses with natural moleculesof biological significance, part II: Grafting of polyphenolsextracted from grape skin. *Appl. Surf. Sci.* **2013**, *287*, 341–348. [CrossRef]

51. Ferraris, S.; Zhang, X.; Prenesti, E.; Corazzari, I.; Turci, F.; Tomatis, M.; Vernè, E. Gallic acid grafting to a ferrimagnetic bioactive glass-ceramic. *J. Non-Crystalline Solids* **2016**, *432*, 167–175. [CrossRef]

52. Yan, X.; Xu, T.; Chen, G.; Yang, S.; Liu, H.; Xue, Q. Preparation and characterization of electrochemically deposited carbon nitride films on silicon substrate. *J. Phys. D Appl. Phys.* **2004**, *37*, 907–913. [CrossRef]

53. Sun, L.; Han, C.; Wu, N.; Wang, B.; Wang, Y. High temperature gas sensing performances of silicon carbide nanosheets with an n–p conductivity transition. *RSC Adv.* **2018**, *8*, 13697–13707. [CrossRef]

54. Fernandes, S.; Sadocco, P.; Alonso-Varona, A.; Palomares, T.; Eceiza, A.; Silvestre, A.J.; Mondragon, I.; Freire, C.S. Bioinspired antimicrobial and biocompatible bacterial cellulose membranes obtained by surface functionalization with aminoalkyl groups. *ACS Appl. Mater. Interfaces* **2013**, *5*, 3290–3297. [CrossRef] [PubMed]

55. De Castro, D.O.; Bras, J.; Gandini, A.; Belgacem, N.; Belgacem, M.N. Surface grafting of cellulose nanocrystals with natural antimicrobial rosin mixture using a green process. *Carbohydr. Polym.* **2016**, *137*, 1–8. [CrossRef] [PubMed]

56. Khanjanzadeh, H.; Behrooz, R.; Bahramifar, N.; Gindl-Altmutter, W.; Bacher, M.; Edler, M.; Griesser, T. Surface chemical functionalization of cellulose nanocrystals by 3-aminopropyltriethoxysilane. *Int. J. Boil. Macromol.* **2018**, *106*, 1288–1296. [CrossRef] [PubMed]

57. Abdel-Naby, A.S.; Al-Ghamdi, A.A. Chemical modification of cellulose acetate by diallylamine. *Int. J. Curr. Microbiol. App. Sci.* **2014**, *3*, 10–24.